Thermoelectric Materials

Guest Editor Andrei Shevelkov
Moscow State University, Russia

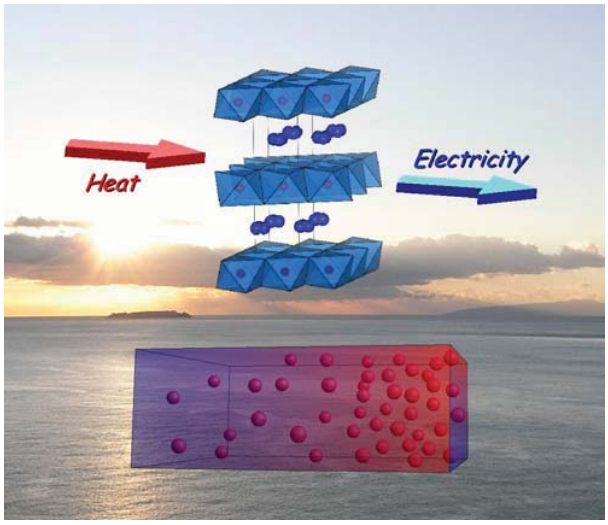

Image reproduced with permission of Ichiro Terasaki

Articles published in this issue include:

PERSPECTIVES:

Thermoelectric clathrates of type I
Mogens Christensen, Simon Johnsen and Bo Brummerstedt Iversen
Dalton Trans., 2010, DOI: 10.1039/b916400f

Wet chemical synthesis and thermoelectric properties of V-VI one- and two-dimensional nanostructures
Genqiang Zhang, Qingxuan Yu and Xiaoguang Li
Dalton Trans., 2010, DOI: 10.1039/b913462j

HOT ARTICLES:

Novel thermoelectric properties of complex transition-metal oxides
Ichiro Terasaki, Manabu Iwakawa, Tomohito Nakano, Akira Tsukuda and Wataru Kobayashi,
Dalton Trans., 2010, DOI: 10.1039/b914661j

Effect of Zn doping on improving crystal quality and thermoelectric properties of borosilicides
Takao Mori, David Berthebaud, Toshiyuki Nishimura, Akiko Nomura, Toetsu Shishido and Kazuo Nakajima, *Dalton Trans.,* 2010, DOI: 10.1039/b916028k

DOI: 10.1039/b914712h

High-temperature transport properties of complex antimonides with *anti*-Th_3P_4 structure

A. Chamoire,[a] F. Gascoin,*†[b] C. Estournès,[b] T. Caillat[c] and J.-C. Tédenac[a]

Polycrystalline samples of R_4Sb_3 (R = La, Ce, Sm and Yb) and $Yb_{4-x}R'_xSb_3$ (R′ = Sm and La) have been quantitatively synthesized by high-temperature reaction. They crystallize in the *anti*-Th_3P_4 structure type ($I\bar{4}3d$, no. 220). Structural and chemical characterizations have been performed by X-ray diffraction and electron microscopy with energy dispersive X-ray analysis. Powders have been densified by spark plasma sintering (SPS) at 1300 °C under 50 MPa of pressure. Transport property measurements show that these compounds are n-type with low Seebeck coefficient except for Yb_4Sb_3 that shows a typical metallic behavior with hole conduction. By partially substituting Yb by a trivalent rare earth we successfully improved the thermoelectric figure of merit of $Yb_{4-x}R'_xSb_3$ up to 0.75 at 1000 °C.

Introduction

With the price of oil spiking, interest in renewable sources of energy has never been as high. One particularly promising technology is the efficient waste heat recovery *via* thermoelectric energy conversion. Indeed, since this technology can be applied to any waste energy streams, from automobile exhaust gas to industrial waste heat associated with many manufacturing processes (forming, melting…), the benefits at stake are enormous. However, this technology can only be economically viable with the discovery of new, more efficient materials.

The quality of a thermoelectric material is estimated by its figure of merit ZT equal to $(\alpha^2/\kappa\rho)T$ where ρ is the electrical resistivity, κ the thermal conductivity (the sum of an electronic (κ_e) and a lattice (κ_l) component), and α the Seebeck coefficient. Good thermoelectric materials must thus have a high Seebeck coefficient, a low electrical resistivity and a low thermal conductivity. Unfortunately, these three variables are interdependent and the improvement of one of them is often counterbalanced by the worsening of the others. The challenge is then to finely tune the transport properties to achieve the best figure of merit. This is usually done by tuning the carrier concentration (between 10^{18} and 10^{20} cm^{-3}) through chemical substitution and doping. Furthermore, research must focus on lowering κ_l, a factor influenced by the complexity of the crystal structure, the constituting elements, and the degree of structural disorder.

Rare-earth chalcogenides crystallizing in the Th_3P_4 structure type have been systematically studied more than twenty years ago.[1] In many of these systems, the existence of a solid solution between R_3X_4 and R_2X_3 (R = lanthanides and X = S, Se and Te) and therefore the presence of a metal–insulator transition permits to easily tune the charge carrier concentration. Consequently, one of the most efficient n-type high-temperature thermoelectric materials known today is a member of the La_3Te_4–La_2Te_3 solid solution and has a ZT higher than 1.0 at temperatures >1000 °C.[2] Consequently, we have chosen to study compounds that crystallize in the *anti*-Th_3P_4 structure types. These structure types are rather ubiquitous amongst rare-earth/p-block element binary systems. More particularly, we will focus on rare-earth antimonides for p-type materials. This "restriction" on the elements to use is based on band structure analysis of rare-earth pnictides, with the antimonides being situated in between the insulator-like arsenides and the metallic-like bismuthides.[3] Thus, this makes the antimonides targets of choice for thermoelectric materials since their properties will be ideally situated between the low Seebeck coefficient and large electronic conductivity of metals and the large Seebeck coefficient and low electrical conductivity of insulators.

In this contribution, we report on the quantitative synthesis of several binary compounds R_4Sb_3 with R = La, Ce, Sm and Yb and on different members of the solid solution $Yb_{4-x}R'_xSb_3$ (R′ = Sm and La), on their densification by spark plasma sintering, and finally on their magnetic and thermoelectric properties. We also discuss the use of the Zintl formalism in order to rationalize the structure–property relationships.

Experimental

Synthesis

All the compounds were prepared directly from the elements by high-temperature synthesis. Stoichiometric mixtures of pure elements (Sb pieces 99.999% Aldrich, La, Ce, Sm and Yb pieces 99.9% REO–Metall Rare Earth Ltd) were directly loaded into 10 mm diameter niobium containers, inside a glove box. These containers were arc-welded shut under argon and in turn enclosed in a fused-silica tube flame-sealed under dynamic secondary vacuum (2–5 × 10^{-6} mbar). These reaction vessels were placed in a tube-furnace, warmed to 1050 °C at a rate of 50 °C h^{-1}, and

[a]*Institut Charles Gerhardt Montpellier, Equipe PMOF, UMR 5253 CNRS-ENSCM-UM2-UM1, Université Montpellier II, 34095, Montpellier, France*
[b]*CIRIMAT, PNF2 MHT, Université Paul Sabatier, 33062, Toulouse, France. E-mail: franck.gascoin@ensicaen.fr*
[c]*Jet Propulsion Laboratory, California Institute of Technology, Pasadena, CA 91109, USA*
† Current address: ENSICAEN CNRS, UMR 6508, Lab CRISMAT, F-14050 Caen 4, France.

maintained at that temperature for 72 h. The ampoules were then removed quickly from the hot furnace and dropped in cold water. Subsequently, the assemblies were placed back in a furnace for an annealing period of 10 days at 900 °C.

Characterization and densification

Phase purities were checked by X-ray diffraction analysis (Philips X'Pert) and the lattice constants refined by the Rietveld method using the program Fullprof[4] on 39 reflections. Composition and microstructure were checked by scanning electron microscopy (SEM) equipped with energy dispersive X-ray spectroscopy (EDX).

All polycrystalline samples were densified using a Dr Sinter 2080 SPS apparatus (SPS Syntex Inc., Tokyo, Japan). About 1 g of powder was first mechanically ground in a planetary ball mill (Fritsch Pulverisette P5) before being loaded into an 8-mm inner diameter cylindrical high density graphite die. The temperature was first automatically raised to 600 °C over a period of 3 min, and from this point on it was monitored and regulated by an optical pyrometer focused on a small hole located at the surface of the die. A heating rate of 50 °C min^{-1} was used to reach the final temperature of 1300 °C at which the sample was kept for 3 min. After this short dwelling time, the temperature was cooled to 600 °C over a period of 15 min. A uniaxial pressure of 50 MPa was applied immediately before and until completion of the temperature step at 1300 °C. During the cooling, the pressure was released slowly in order to avoid too much mechanical stress on the sample. In these conditions, during the sintering cycle, the current passing through the die and the voltage reached maximum values of 348 A and 3.4 V, respectively.

Magnetic and transport property measurements

Magnetic susceptibility was measured from 2 K to room temperature using a SQUID magnetometer from Quantum Design under a constant magnetic field of 5000 G. Electrical resistivity (ρ) was measured using the van der Pauw technique with a current of 100 mA.[5] The Seebeck coefficient (α) was measured with a light pipe technique with a W/Nb thermocouple[6] and the thermal conductivity (κ) was directly deduced from simultaneous measurements of thermal diffusivity and specific heat using the laser flash method. All properties are measured as a function of temperature under vacuum (from room temperature to 1000 °C).

Results and discussion

Binaries R_4Sb_3

Structure and characterization. Binary compounds La_4Sb_3, Ce_4Sb_3, Sm_4Sb_3 and Yb_4Sb_3 crystallize in the *anti*-Th_3P_4 structure type ($I\bar{4}3d$, no. 220, $Z = 4$). In this cubic structural arrangement the antimony atoms occupy the 12a Wyckoff position and are eight-coordinated by two interpenetrated ytterbium tetrahedra forming a bis-disphenoid. Ytterbium atoms are in 16c Wyckoff position and they lie in the center of a distorted octahedron of antimony. Furthermore, interstitial sites are in 12b Wyckoff positions and are surrounded by two interpenetrated Sb and Yb tetrahedra that form a distorted square antiprism. Powder X-ray diffraction studies confirmed that the cell parameter a = 9.649, 9.508, 9.308 and 9.321 Å, for La_4Sb_3, Ce_4Sb_3, Sm_4Sb_3 and Yb_4Sb_3, respectively, are in good agreement with those determined in previous work.[7-10] A five month aging study performed on the four compounds indicates that these materials are stable in air with only few signs of amorphization observed by XRD analysis. Thermogravimetric analysis also demonstrates that these antimonides are stable at high temperature under inert atmosphere or vacuum since they did not degrade up to 1300 °C. This rather refractory character is mainly due to the ionic character of such polar intermetallics, the cohesion of the structure being assured by strong electrostatic forces. In fact, such rare-earth antimonides could be described as Zintl phases, the rare earth elements donating their outer electrons to the antimony atoms to give closed-shell structures. In a more descriptive way, their formula can be written using the Zintl formalism as $4R^{x+} + 3Sb^{3-}$, the electroneutrality being achieved by the presence of extra holes or electrons depending on the charge of the rare earth cation. If the cation is trivalent, there are three extra electrons delocalized over the whole structure ($4R^{3+} + 3Sb^{3-} + 3e^-$), thus forming an n-type material while if the cation is divalent, there is one extra hole delocalized over the whole structure ($4R^{2+} + 3Sb^{3-} + 1h^+$), leading to a p-type conduction. The same formalism has been used for thermoelectric materials such as Mg_3Sb_2 and $Ca_xYb_{1-x}Zn_2Sb_2$,[11] $YbSb_2Te_4$,[12] or $Yb_{14}MnSb_{11}$ and its derivatives.[13] It represents an interesting tool to help choosing the doping agent or the substitution to use to adjust the carrier concentration in the aim of improving the thermoelectric properties.

Transport properties

Except for La_4Sb_3 all measurements have been made up to 1000 °C. The room-temperature Seebeck coefficients of La_4Sb_3, Sm_4Sb_3 and Yb_4Sb_3 are in good agreement with those previously reported.[14] La_4Sb_3, Ce_4Sb_3 and Sm_4Sb_3 have a negative Seebeck coefficient, providing proof of an n-type behavior consistent with the presence of extra delocalized electrons as described above using the Zintl formalism to assign the charges; their values are very low and almost temperature independent from room temperature up to 1000 °C, typical characteristics of the thermopower of metals (Fig. 1). In contrast, the Seebeck coefficient of Yb_4Sb_3 increases linearly with temperature and suggests a p-type behavior from 250 up to 1000 °C where it reaches 70 μV K^{-1}, much higher than that of a metal. The room-temperature electrical resistivity of 0.22 mΩ cm compares very well with the value of 0.2 mΩ cm measured on a single crystal.[15] It increases linearly with temperature and reaches 1.25 mΩ cm at 1000 °C. These results show that Yb_4Sb_3 is rather a semi-metal or a heavily doped semiconductor and its behavior seems similar to that of the most "metallic" member of the solid solution La_3Te_4–La_2Te_3.[2] With such a similarity, it is reasonable to believe that the transport properties of Yb_4Sb_3 can be improved by tuning the carrier concentration.

Magnetic susceptibility

The molar magnetic susceptibility of Yb_4Sb_3 ($\chi = M/H$, normalized per Yb) is in quite good agreement with previous work. Yb_4Sb_3 shows a typical valence fluctuating behavior with a maximum of the susceptibility at 240 K. Since the $\chi^{-1} = f(T)$ data strongly deviate from a straight line, a modified Curie–Weiss

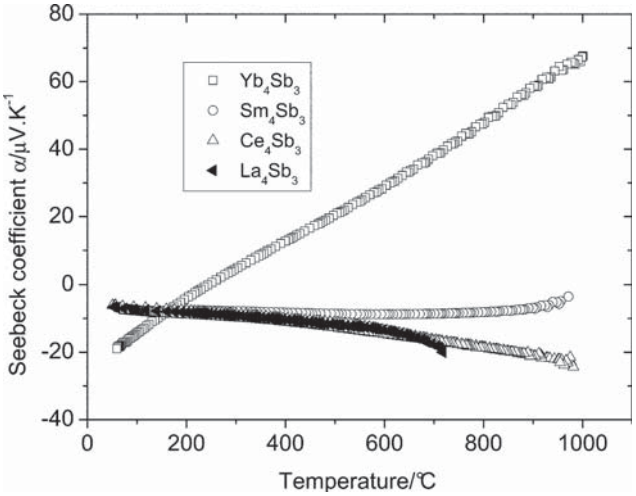

Fig. 1 Seebeck coefficient of L_4Sb_3 (L = Yb, Sm, Ce and La) as a function of temperature.

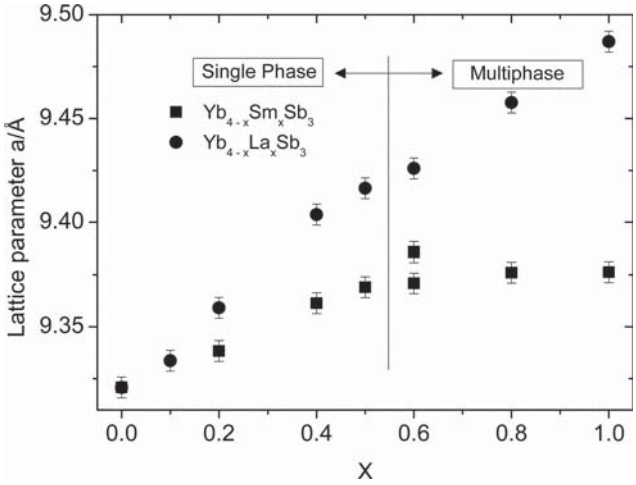

Fig. 2 Lattice parameter a as a function of x in $Yb_{4-x}L_xSb_3$ (L = Sm or La).

law, $\chi(T) = C/(T - \theta_p) + \chi_0$, was used to fit the low-temperature data; χ_0 is the sum of the temperature-independent contribution, *e.g.* van Vleck contribution paramagnetism due to conduction electrons, and core electron diamagnetism, C is the Curie constant and θ_p is the Weiss temperature. We find an effective moment of 0.386 μ_B per Yb which is much lower than the value expected for a free Yb^{3+} ion ($^2F_{7/2}$, $\mu_{eff} = 4.54\ \mu_B$). Thus Yb appears to exist in two valence states, Yb^{2+} and Yb^{3+}. Since Yb^{2+} has ground state $^1S_0$, its resulting effective moment is 0. Then the fraction of each ion can be estimated by using the expression $\mu_{eff} = \sqrt{(1-y)\mu_{eff(Yb^{2+})}{}^2 + y\mu_{eff(Yb^{3+})}{}^2}$ where y is the fraction of Yb^{3+}. Solving this equation with respect to y, we find that in Yb_4Sb_3, ytterbium is mainly divalent with only about 0.8% of Yb^{3+} which is rather low compared to previous measurements made on single crystals.[16] This gives a mean valence of the rare earth element of about 2.01. If we consider the Zintl formalism, we can estimate that Yb_4Sb_3 is electron deficient with 3.88 holes per unit cell, in good agreement with transport property measurements that indicate a p-type behavior. Therefore, the substitution of a divalent ytterbium atom by a trivalent or a tetravalent rare earth should reduce the charge carrier density and improve the thermoelectric properties through the increase of the thermopower.

Solid solutions $Yb_{4-x}Sm_xSb_3$ and $Yb_{4-x}La_xSb_3$

Characterization. We have been able to substitute Yb by Sm up to $x = 0.6$ and by La up to $x = 1$. As expected, in both cases the lattice constant, refined using the Rietveld method, increases linearly with substituent content. In $Yb_{4-x}Sm_xSb_3$ it increases from 9.321 up to 9.385 Å for $x = 0.6$ and in $Yb_{4-x}La_xSb_3$ it reaches 9.487 Å for $x = 1$ (Fig. 2). In both systems, the difficulty to obtain pure samples increases with increasing value of x. Consequently, the synthesis requires rather long annealing periods to remove secondary phases of the rock salt type $Yb_xR_{1-x}Sb$. In fact XRD and SEM analysis confirm the presence of this impurity for values of x as low as 0.6.

Magnetic susceptibility

$Yb_{4-x}La_xSb_3$. Measurements of the temperature dependence of the magnetic susceptibility of $Yb_{4-x}La_xSb_3$ indicate that the magnitude of the susceptibility is not much affected by substitution except at low temperature. However, in this regime it increases by about three orders of magnitude indicating an increase of the quantity of magnetic rare earth. At higher temperature, the susceptibility increases slightly for $x_{La} = 0.2$, that shows a valence fluctuation behavior with a maximum around 200 K. Increasing further the La content, the susceptibility slowly decreases and shows a typical Curie–Weiss paramagnetic behaviour and the valence fluctuation seems to disappear. It must also be taken into account that by increasing the lanthanum content, the additional phase $La_{1-x}Yb_xSb$, containing some Yb^{3+}, starts to form when $x = 0.6$. This could also contribute to the slight increase of Yb^{3+} content at low temperature.

La is a trivalent rare earth and its ground state is $^1S_0$, giving an effective moment $\mu_{eff} = 0$. For the composition $Yb_{4-x}La_xSb_3$ each cationic site is occupied by $(x/4)$ La ions and $(4 - x)/4$ Yb ions. We can estimate the fraction of each Yb ion using $\mu_{eff} = \sqrt{((1-(x/4)-y))\mu_{eff(Yb^{2+})}{}^2 + y\mu_{eff(Yb^{3+})}{}^2 + (x/4)\mu_{eff(La^{3+})}{}^2}$ where x represents La content and y the fraction of Yb^{3+}. This expression can be simplified by replacing μ_{eff} by the known values for the elements and thus appears to be only a function of Yb^{3+} fraction: $\mu_{eff} = \sqrt{y\mu_{eff(Yb^{3+})}{}^2}$. By fitting the low-temperature data with a modified Curie–Weiss law defined previously and solving the equation with respect to y, we obtain the results gathered in Table 1.

As we can see, the Yb^{3+} content oscillates between 0.4 and 1.45% depending on the lanthanum content, values that compare very well with the 0.8% of Yb^{3+} found in the binary Yb_4Sb_3. Considering experimental uncertainties, as well as approximations in calculations, it is reasonable to consider the Yb^{3+} content as almost constant. To conclude, the compound with the highest lanthanum content that could be obtained as a pure phase is $Yb_{3.5}La_{0.5}Sb_3$. Coupling the magnetic measurements results and

Table 1 Parameters obtained from magnetic susceptibility measurements of $Yb_{4-x}La_xSb_3$

% Substitution	μ_{eff}	% La^{3+}	% Yb^{2+}	% Yb^{3+}	Mean valence
5% ($x = 0.2$)	0.336	5	94.56	0.44	2.05
10% ($x = 0.4$)	0.414	10	89.4	0.6	2.11
12.5% ($x = 0.5$)	0.487	12.5	86.35	1.15	2.14
15% ($x = 0.6$)	0.434	15	84.09	0.91	2.16
20% ($x = 0.8$)	0.422	20	79.14	0.86	2.21
25% ($x = 1$)	0.546	25	73.55	1.45	2.26

the Zintl formalism, it can be estimated a formal charge carrier density corresponds to approximately 1.76 holes per unit cell.

$Yb_{4-x}Sm_xSb_3$. Measurements of the temperature dependence of the magnetic susceptibility of $Yb_{4-x}Sm_xSb_3$ indicate that the magnitude of the susceptibility is only slightly affected by the substitution. At low temperature, it increases up to three orders of magnitude for $x_{Sm} = 0.6$ and we observe also a small increase of the susceptibility as a function of Sm content up to $x_{Sm} = 0.6$. In the same way as the lattice constant evolution, the different results observed for $x_{Sm} = 0.6$ are linked to the formation of the second phase. So in this case, the observed behaviour is mainly influenced by the presence of the second phase $Yb_xSm_{1-x}Sb$ in which Yb and Sm are mainly trivalent. We can also note that for compositions with $x = 0.1$ and 0.2 there is a valence fluctuating behaviour denoted by a maximum of the magnetic susceptibility around 200 K, a trend that completely disappears for $x = 0.4$. The valence of rare earth in these solid solutions is much more difficult to determine by magnetic measurement only. Indeed Sm can exhibit both +2 and +3 valences. Sm^{2+} ($^7F_0$) has no effective moment while Sm^{3+} ($^6H_{5/2}$) presents an effective moment of about 0.85 μ_B per Sm at 0 K. Consequently we are able to only estimate Yb^{3+} content as a function of Sm^{3+} content. Thus, for the composition $Yb_{4-x}Sm_xSb_3$ a cationic site is occupied by $x/4$ Sm ions and $(4 - x)/4$ Yb ions. Then we can estimate the fraction range of each ion (Yb^{3+} and Sm^{3+}) using the expression

$$\mu_{eff} = \sqrt{((1-(x/4)-y))\mu_{eff(Yb^{2+})}{}^2 + y\mu_{eff(Yb^{3+})}{}^2 + z\mu_{eff(Sm^{3+})}{}^2 + ((x/4)-z)\mu_{eff(Sm^{2+})}{}^2}$$

where x represents Sm content, and y and z are the proportions of Yb^{3+} and Sm^{3+}, respectively. We finally obtain the general expression: $\mu_{eff}{}^2 = (4.54)^2y + (0.85)^2z$.

The results obtained from experimental data are gathered in Table 2. It should be mentioned here that there are two samples corresponding to a 15% substitution (or $x = 0.6$). One of them is pure (and referred as monophasic in the table), the other contains impurities and is referred as biphasic in the table). We are convinced that this difference is due to the fact that for a high percentage of substitution, the synthesis parameters (and mostly the annealing step) are determining the purity of the sample and that slight changes can lead to the precipitation of impurities.

Table 2 Parameters obtained from magnetic susceptibility measurements of $Yb_{4-x}Sm_xSb_3$

% substitution	μ_{eff}	% Sm^{3+}	% Yb^{2+}	% Yb^{3+}	Mean valence
Monophase					
2.5% ($x = 0.1$)	0.523	2.5	96.27	1.23	2.04
5% ($x = 0.2$)	0.388	5	94.45	0.55	2.055
10% ($x = 0.4$)	0.590	10	89.58	1.33	2.13
15% ($x = 0.6$)	1.21	15	78.45	6.55	2.21
Biphase					
15% ($x = 0.6$)	0.917	15	82.45	2.55	2.17
20% ($x = 0.8$)	0.975	20	76.09	3.91	2.24
25% ($x = 1$)	0.984	25	71.18	3.82	2.29

We can see that Yb^{3+} content is not much affected by the substitution up to $x_{Sm} = 0.4$ and variations of Sm^{3+} content do not show a strong influence on Yb^{3+} content. It increases much more when the Sm content is increased to $x = 0.6$ and above and this is due to the formation of the additional phase $Sm_{1-x}Yb_xSb$ in which the ytterbium is trivalent. Thus, with increasing Sm content the overall mean valence of the rare earth is increased and the formal densities of carrier should be reduced from 3.88 in Yb_4Sb_3 to 1.92 in $Yb_{3.6}Sm_{0.4}Sb_3$.

It should be mentioned and emphasized that our interpretations do not take into account the change of effective magnetic moment (of Yb or Sm) with temperature. Furthermore, we are aware that fitting low-temperature data with a Curie–Weiss law may only reflect the presence of Yb^{3+} impurities, indeed the presence of a Curie tail at low temperature may merely reflect the presence of ytterbium oxide or of YbSb, a compound that we clearly detect for high substitution rate. Nonetheless, for substitution up to $x_{Sm} = 0.4$ and $x_{La} = 0.5$, we can conclude that the mean valence of the rare earth element is higher than in Yb_4Sb_3. This is due to the substitution of the divalent ytterbium by a trivalent samarium or lanthanum atom while the Yb^{3+} content (whether contained in the antimonides or in impurity phases) stays constant and relatively small. Therefore with increased substitution by trivalent samarium or lanthanum, the hole concentration should be increased, and should result in the enhancement of the thermoelectric properties through the increase of the Seebeck coefficient.

Transport properties

Transport property measurements have been performed for $Yb_{4-x}Sm_xSb_3$ ($x = 0.2, 0.4$) and $Yb_{4-x}La_xSb_3$ ($x = 0.1, 0.2, 0.5$) as a function of the temperature and compared with those of Yb_4Sb_3. For both substituents, the Seebeck coefficient varies linearly with increasing temperature. As the carrier concentration is lowered by the increasing content x of trivalent rare earth (La or Sm), the Seebeck coefficient increases with x until it reaches 120 μV K^{-1} for $Yb_{3.6}Sm_{0.4}Sb_3$ and $Yb_{3.5}La_{0.5}Sb_3$, which have almost twice the thermopower of the binary compound Yb_4Sb_3 (Fig. 3). Electrical resistivity is not so much affected by substitution and stays quite low. It increases slightly for the most substituted solid solutions members and reaches 1.38 mΩ cm for $x_{Sm} = 0.4$ and 1.51 mΩ cm for $x_{La} = 0.5$ at 1000 °C (Fig. 4), again in good agreement with the carrier concentration decrease. Thermal conductivity is also relatively low and all substituted compounds show similar variations with a maximum around 200 °C and a linear decrease with increasing temperature. For samarium substituted compounds the thermal conductivity decreases linearly from about 40 mW cm^{-1} K^{-1} at 200 °C down to 20–25 mW cm^{-1} K^{-1} at 1000 °C. La substitution gives even lower thermal conductivities, for $Yb_{3.5}La_{0.5}Sb_3$, it has a maximum of 23 mW cm^{-1} K^{-1} at 200 °C and decreases down to 16 mW cm^{-1} K^{-1} at 1000 °C (Fig. 5). These rather low values could be explained by the higher weight difference between Yb and La than between Yb and Sm, thus disrupting more efficiently the phonon mean free path. The dimensionless thermoelectric figures

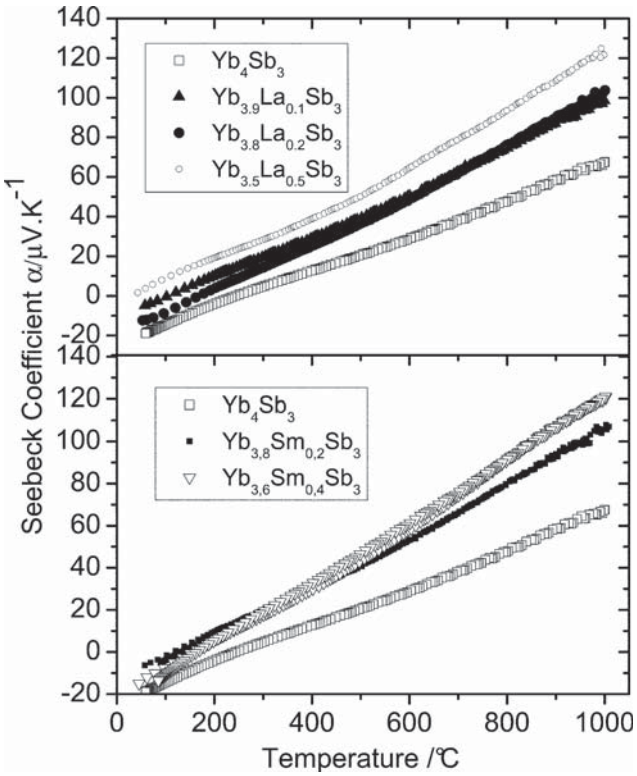

Fig. 3 Seebeck coefficient as a function of temperature for $Yb_{4-x}L'_xSb_3$ (L′ = Sm or La).

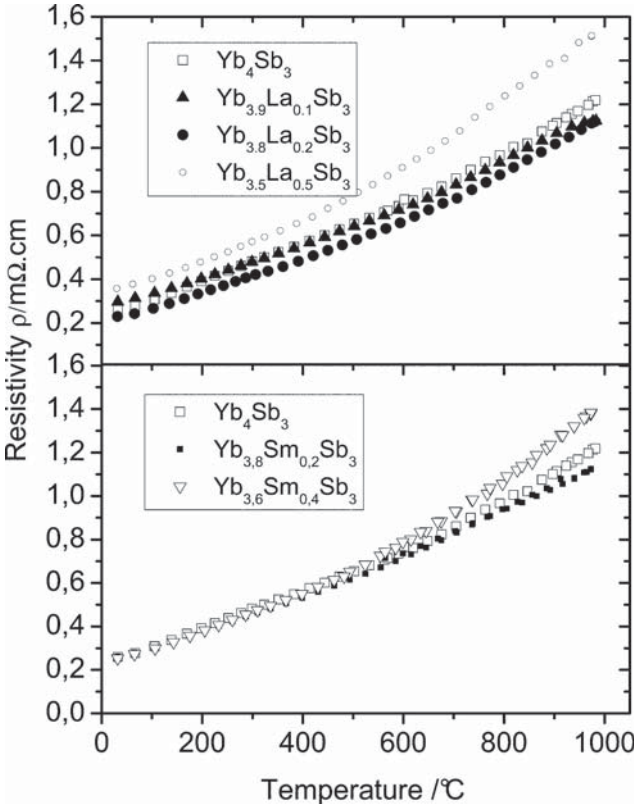

Fig. 4 Electrical resistivity as a function of temperature for $Yb_{4-x}L'_xSb_3$ (L′ = Sm or La).

of merit ZT can calculated using the data reported here. The curves in Fig. 6 are generated using polynomial fits to the raw data for the Seebeck coefficient, the thermal and electrical conductivity. No extrapolation is utilized in generating ZT. The figures of merit increase sharply with increasing temperature. Despite the fairly low degree of substitution ($x_{Sm} = 0.4$ and $x_{La} = 0.5$) a maximum ZT of ~0.75 at 1000 °C is obtained for $Yb_{3.5}La_{0.5}Sb_3$ (Fig. 6) and a slightly lower value is reached for $Yb_{3.6}Sm_{0.4}Sb_3$. These values render these rare earth antimonides competitive for very high-temperature applications or at least justify further investigations. Moreover, the family of antimonide compounds crystallizing in the *anti*-Th_3P_4 structure type is almost unlimited and should lead to the discovery of even more efficient thermoelectric materials.

Conclusions

Yb_4Sb_3 and the solid solutions $Yb_{4-x}R_xSb_3$ with R = Sm and La were studied. The high-temperature synthesis we used allowed us to produce pure samples up to $x = 0.5$–0.6, above this value, the pseudo-binary rock salt type compounds ($Yb_xR_{1-x}Sb$) start to form. The binary compound Yb_4Sb_3 has rather poor thermoelectric properties as it remains "too metallic". As anticipated, and in good agreement with the magnetic measurements, the substitution of divalent Yb by trivalent Sm or La improves the thermoelectric properties of the solid solution members. In fact, through the lowering of the carrier concentration, the Seebeck coefficient increases and is almost doubled while the electrical resistivity increases to a much lower extent. Furthermore, the mixture of two cations of different size, weight, and charge increases the disorder, and thus decrease the thermal conductivity to a fairly

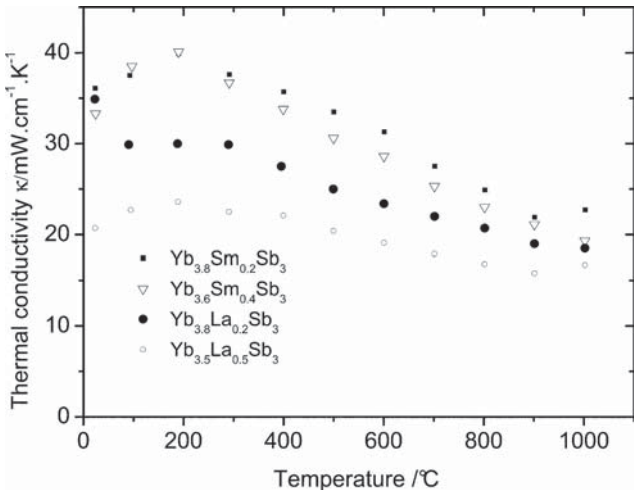

Fig. 5 Thermal conductivity as a function of temperature for $Yb_{4-x}L'_xSb_3$ (L′ = Sm or La).

low value. Consequently, the largest thermoelectric figure of merit is $ZT = 0.75$ at 1000 °C for $Yb_{3.5}La_{0.5}Sb_3$. Such antimonides, with little improvement, could therefore be useful for high-temperature thermoelectric applications. Work to increase further the thermopower of such phases is underway. Investigations are under way to evaluate other types of substitutions as well as the possibilities to partially fill the interstitial sites.

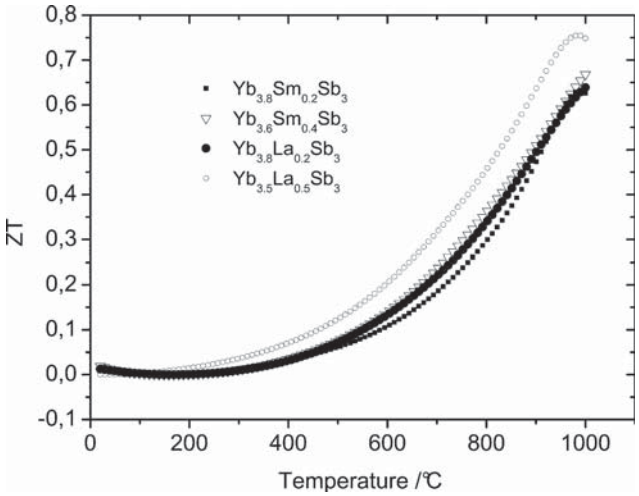

Fig. 6 Thermoelectric figure of merit ZT as a function of temperature for $Yb_{4-x}L'_xSb_3$ (L′ = Sm or La).

Acknowledgements

The authors would like to thank the financial support of the "Agence Nationale pour la Recherche", project ANR-JCJC06-1355090. The help of C. Rebel for the magnetic measurements is also acknowledged.

References

1 K. A. Jr Gschneidner, J. F. Nakahara, B. J. Beaudry and T. Takeshita, *Mater. Res. Soc. Symp. Proc.*, 1987, **97**, 359; C. Wood, *Rep. Prog. Phys.*, 1988, **51**, 459.

2 L. R. Danielson, M. N. Alexander, C. Vining, R. A. Lockwood and C. Wood, Seventh International Conference on Thermoelectric Energy Conversion, Arlington, TX, March 1988, 16–18, p. 71; A. May, J. Snyder, J.-P. Fleurial, Space Technology and Applications International Forum 2008, ed. M. S. El-Genk, p. 672; A. F. May, D. J. Singh and G. J. Snyder, *Phys. Rev. B: Condens. Matter Mater. Phys.*, 2009, **79**, 153101; A. F. May, J.-P. Fleurial and G. J. Snyder, *Phys. Rev. B: Condens. Matter Mater. Phys.*, 2008, **78**, 125205.

3 V. N. Antonov, B. N. Harmon and A. N. Yaresko, *Phys. Rev. B: Condens. Matter Mater. Phys.*, 2005, **72**, 085119.

4 J. A. McCormack and J. P. Fleurial, *Mater. Res. Soc. Symp. Proc.*, 1991, **234**, 135.

5 C. Wood, D. Zoltan and G. Stapfer, *Rev. Sci. Instrum.*, 1985, **56**, 719.

6 J. Rodriguez-Carvajal, Fullprof, *Phys. B*, 1993, **192**, 55.

7 R. J. Gambino, *J. Less Common Met.*, 1967, **12**, 344.

8 R. E. Bodnar and H. Steinfink, *Inorg. Chem.*, 1967, **6**, 327.

9 Y. Wang, L. D. Calvert and J. B. Taylor, *Acta Crystallogr., Sect. B: Struct. Crystallogr. Cryst. Chem.*, 1980, **36**, 221.

10 A. Ochiai, S. Nakai, A. Oyamada, T. Suzuki and T. Kasuya, *J. Magn. Magn. Mater.*, 1985, **47–48**, 570.

11 C. L. Condron, F. Gascoin, G. J. Snyder and S. M. Kauzlarich, *J. Solid State Chem.*, 2006, **179**, 2252; F. Gascoin, S. Ottensmann, D. Stark, S. M. Haile and G. J. Snyder, *Adv. Funct. Mater.*, 2005, **15**, 1860.

12 A. Guloy, A. Chamoire, J.-C. Tedenac, F. Gascoin and G. J. Snyder, *Phys. Status Solidi RRL*, 2007, **1**, 265.

13 S. Brown, F. Gascoin, G. J. Snyder and S. M. Kauzlarich, *Chem. Mater.*, 2006, **18**, 1873; S. R. Brown, E. Toberer, T. Okeda, C. Cox, F. Gascoin, S. M. Kauzlarich and G. J. Snyder, *Chem. Mater.*, 2008, **20**, 3412; C. A. Cox, E. S. Toberer, A. A. Levchenko, S. R. Brown, G. J. Snyder, A. Navrotsky and S. M. Kauzlarich, *Chem. Mater.*, 2009, **21**, 1354; E. S. Toberer, C. A. Cox, S. R. Brown, T. Ikeda, A. F. May, S. M. Kauzlarich and G. J. Snyder, *Adv. Funct. Mater.*, 2008, **18**, 2795; E. S. Toberer, S. R. Brown, T. Ikeda, S. M. Kauzlarich and G. J. Snyder, *Appl. Phys. Lett.*, 2008, **93**, 062110.

14 E. Bucher, A. S. Cooper, D. Jaccard and J. Sierro, *Valence Instabilities and Related Narrow Band Phenomena*, ed. R. D. Parks, Plenum, New York, 1977, p. 529.

15 A. Ochiai, T. Suzuki and T. Kasuya, *J. Phys. Soc. Jpn.*, 1990, **59**, 4129.

16 S. Suga, S. Ogawa, H. Namatame, M. Tanigushi, A. Kakizaki, T. Ishii, A. Fujimori, S. Oh, H. Kato, T. Miyahara, A. Ochiai, T. Suzuki and T. Kasuya, *J. Phys. Soc. Jpn.*, 1989, **58**, 4534.